Nucleation of naturally occurring calcic amphibole asbestos

Maxime Misseri

Title e

Nucleation of naturally occurring calcic amphibole asbestos

Author

Maxime Misseri[1]

[1]Sorbonne University, UTC, EA 4297 UTC/ESCOM, F-60205 Compiègne cedex,
ORCID https://orcid.org/0000-0003-2606-2122

E-mail : maxime.misseri@ad-lab.frr

Abstract

This article proposes an initial model of natural asbestiform minerals growing in four stages. Structures dating from the early stages of the development were observed in the damaged zone surrounding meso-fractures, more particularly in microfractures, microcavities and microcracks that lie in front of and along mesofractures. This study is limited to calcium amphiboles cross-fibers, which develop from altered calcium amphiboles. The observations were made using PLM, with some using TEM. The samples are amphibolites, dolerites and skarns from France. All these rocks have in common that they have been exposed to hydrothermal circulation which gives them a propylite character. The earliest phenomenon was the development of metasomatic veins. In these veins, actinolite form pseudomorphs after hornblendes. The new amphiboles preserve the original morphology of hornblende, in particular the appearance of the cleavages. In the second stage, hydrothermal Fluid circulation promotes the development of subgrains (DSG) with boundaries generally parallel to the cleavage. Some sub-grains become thinner and more and more individualized due to dissolution by the hydrothermal fluid. The third stage is fracturing. The irregular ends of DSGs and amphibole debris can form the substrate of asbestiform mineral nuclei.

Further dissolution of DSGs can also lead to the creation of substrates. The last stage is the nucleation and growth. The nuclei have a conical shape and variable widths, from a few microns to about ten microns. The basal parts of the asbestos minerals (BPAMs) extend the DSGs along the c axis. BPAMs have variable widths and can divide during their development at the level of transverse microcracks. BPAMs when not dividing have a morphology comparable to that of whisker nanocrystals synthesized using the vapour-liquid-crystal mechanism. The shape of the fragments from BPMAs is close to that of DSGs as both have variable widths and both have lengths controlled by microcracks.

Keywords

Nucleation, calcic amphibole, natural occurred asbestos, damage zone,

1. Introduction

Asbestos is a commercial term that refers to a group of naturally-occurring minerals. These include chrysotile, belonging to the serpentine family, and amphiboles formed in an asbestiform habit: grunerite (amosite), riebeckite (crocidolite), actinolite, tremolite and anthophyllite. In nature, the same amphiboles may also form in a non-asbestiform habit (acicular or prismatic). In such cases, these minerals produce cleavage fragments when subjected to mechanical stress. These are elongated mineral particles that form preferentially along crystal weakness planes, cleavages (110), monoclinic amphiboles and (210) orthorhombic amphiboles.

Standards for counting airborne asbestos fibers by phase contrast microscopy (PCM), based on World Health Organization recommendations (WH0, 1997), do not differentiate cleavage fragments from asbestiform mineral particles. The same is true of all standards for counting airborne fibers by transmission electron microscopy (TEM)

(French standard NF X 43 050, 2021; ISO 13794, 2019; ISO 10312, 2019) and by scanning electron microscopy (ISO 14966, 2019).

Many regulations around the world, especially those in European Union countries, believe that only asbestos fibers with their CAS number as a reference should be counted. The CAS registry does not, however, describe either the structure of asbestos amphiboles or a testing method. Since asbestos testing in the natural environment is less regulated and standardized, laboratory testing is often responsible for the choice of method to characterize asbestiform amphiboles. Environmental Protection Agency (EPA) and Health, Safety and Environment (HSE) method criteria (EPA, 1993; HSG 248, 2021) are generally used to observe hand samples of rock and soil and for observations by polarized light microscopy (PLM). The standard (ISO 22262-1, 2012) provides for differentiation by PLM and some provisions can be used in TEM and SEM. Differentiation can be done with procedures based on: the study of the aspect ratios of a population of particles, applicable in PLM, PCM, TEM and SEM (BAILEY et al., 2004); the study of a population of particles taking into consideration the width and aspect ratio, applicable in TEM (CHATFIELD, 2008); the width of particles, applicable in TEM and SEM (STANTON et al., 1981 and VAN ORDEN et al., 2009) also applicable in PCM (HARPER et al., 2008); and on morphological criteria and criteria obtained from TEM observation using a flowchart (R.J. Lee in BERMAN, 2003 and VAN ORDEN et al., 2008). The MP2015 flowchart called MP 2015 (MISSERI et al., 2021) was put forward to get comparable results between analyses done by TEM and PLM. In the natural environment, flow charts are essential for counting and identifying fibers in air, rock and soil containing little asbestos, especially in regions where there is no threshold or a very low threshold. Whatever the method, it is difficult to differentiate particles of asbestiform and non-

asbestiform amphiboles when the aspect ratio is between 5:1 and 20: 1. Better understanding of the geological circumstances that preferentially produce these fibrous minerals can help differentiate particles produced and, in all cases, help improve interpretation of analysis results.

In this study, we will try to reconstruct the process of asbestos fiber formation by tracing the mineral record of the geological stages that led some amphiboles to evolve and contribute to the emergence of asbestiform amphiboles.

The fiber nucleation zones in asbestos-containing veins are particularly useful in examining this topic. Minerals in the wallrock of the veins are generally dissolved by hydrothermal fluid and redeposited nearby in the form of asbestos amphibole (VAN DER WEL, 1972). This mechanism was described for the formation of chrysotile (ANDREANI, 2005), actinolite from pyroxene (VIGNARO, 2020). In these zones, we can observe the Basal Parts of Asbestiform Minerals (BPAMs), which can be thicker than their extremities. Here, hydrothermal fluids isolate subgrains in wallrock amphiboles. Their boundaries are cleavage planes (110) in the beginning. These subgrains vary greatly in width. Some can be very thin, less than one micron, due to intragrain hydrothermal circulation. The extremities of these subgrains form the substrate for asbestiform mineral nuclei. Under mechanical stress, altered amphibole Developing SubGrains (DSGs) can release particular cleavage fragments with morphologies similar to those of asbestos fibers. From a geological perspective, the boundary between these two minerals can be differentiated by microscopy: DSGs are produced by dissolution and asbestiform minerals are the result of preferential crystal growth along the axis [001]. It is difficult, but not impossible, to differentiate between cleavages from DSGs and particles from BPAMs in laboratory testing The effect on health of fragments from these

mineral parts, DSGs from the dissolution of an amphibole and BPAMs which is the basal part of an amphibole with a particular growth, has not yet been studied.

2. Material and methods

2.1. Material

The study is limited to the observation of calcium amphiboles that are found in cross-fiber asbestos veins, in damage zone microfractures and microcavities near these veins. The rocks studied are metasomatic (propylites). Propylites (VON RICHTHOFEN, 1868) are metasomatic greenstones. Low-temperature propylites contain calcite, chlorite, quartz and pyrite. Higher-temperature propylites (280-350°C) contain epidote, actinolite, biotite and magnetite (ZHARIKOV et al., 2007, and LAGAT 2009). There are classifications of damage zones around faults that can be found in the field (KIM, 2004; CHOI 2012, PEACOCK 2017). These classifications are difficult to use in their entirety, given the scale on which the work was done and also depending on the structures studied. This paper only looks at extension microstructures of several microns as well as their position in relation to mesofractures of several millimeters. The relationships between mesostructures and larger structures are not described. Observations are limited to microstructures and mesostructures as defined by Mohammednejad's adaptation of the Van Mier scale (VAN MIER, 1996; MOHAMMADNEJAD, 2021). When a mesoscopic fracture propagates, there is also a succession of microfractures, microcavities and microcracks. Microfractures, microcavities and microcracks are located at the front of the "nose" of the mesofracture in the propagation zone and around the edges of the fracture (BAZANT, 2003; MOHAMMADNEJAD, 2021). The progression of the fractures and microcavities is fossilized in these damage zones.

This is also the case for the inflow of hydrothermal fluids inside these openings. By studying them, we can observe the origin of asbestos fibers.

Samples were chosen in order to examine the different phases of asbestos fiber formation: metasomatic veins (A), individualization of subgrains, the extremities of which form the substrate for nuclei (B), fracturing (C), and the start of fiber growth (D). Samples may contain traces of the entire process or just one part of it.

The observations were made by PLM, with some by TEM. The samples (Table 1) analyzed by PLM are amphibolites from Corsica and the Alps, dolerites from the Vendee department, and skarns from the Pyrenees. Special attention was paid to microfractures (from several microns to several millimeters in width) made up of minerals showing evidence of hydrothermal activity and microcavities of several microns. Two types of mineral structures that are generally not considered in the study of asbestiform minerals are described, but not studied crystallographically.

A sample of New Caledonia greenschist and a sample of asphalt road aggregate were analyzed by TEM (Table 1) to round out the descriptions.

An additional sample (Table 1) of amphibolite from the Limousin region was analyzed by PLM to illustrate a discussion point.

Ech.	Source	Phase A Figure	Phase B figure	Phase C figure	Phase D figure	Type of fracture	PLM or TEM
ALP 1	Alps, Belledone Massif	1a	1a	1a		Along a meso-fracture	PLM
ALP 2	Alps, Belledone Massif			1b	1b	Along a meso-fracture	PLM
COR	Corsica cap	2a	2b , 2c	2d,2e	2f, 2g, 2h	Around a meso-fracture pit	PLM
VEN	Vendee, Armorican Massif				3a, 3b,3c,3d	Along a meso-fracture	PLM
PYR	Pyrenees, Saleau mine		4a		4b, 4c,4 d	Undetermined	PLM
Lim	Limousin, Central Massif		6			Undetermined	PLM
NC	Greenschist, N^{lle} Caledonie				5a	Undetermined	TEM
GR	Asphalt road aggregate				5b	Undetermined	TEM

Table 1 : Origin of samples and location of structures of interest photographed versus meso-fractures

2.2. Polarized Light Microscopy (PLM)

Samples of coherent rock that were thought to include metasomatic rocks (propylites) or that contained hydrothermal veins, were selected. The analysis protocol was based on creating thin sections to be observed under Polarized Light Microscopy (PLM). A Leica DM750P microscope was used. Observations were made at 100x or 400x magnification. The thin sections were analyzed petrographically. The microscope was used to determine the type of parent rock and alteration minerals, to track the mineralogical evolution of the alteration minerals and to describe the early asbestiform mineral growth stages.

2.3. Transmission Electron Microscope (TEM)

The methodology and equipment were described in an earlier article (MISSERI 2018). A short description of the method is given next. The rock is crushed. About 90% of the particles, after manual grinding, had a diameter of less than 50 µm. The subsample prepared for TEM analysis was suspended in 50 ml of deionized water. Dilution was adjusted according to the transparency to obtain less than 20% electron-dense material on the grids. The vial was submitted to ultrasound for 1 min. The preparation of the TEM grid used the drop-mount technique. The TEM-EDS analyses were performed using a FEI CM200 equipped with a calibrated SAMx NumeriX EDS.

Two particles that were analyzed by TEM were chosen to round out the PLM thin section observations.

3. Results and discussion

3.1. Results from PLM observations

The first example (samples ALP1 and ALP2) is a plagioclase amphibolite that comes from the Allemont formation in the Belledonne mountain range, in the Alps. In sample ALP1, the rock is primarily made up of green hornblende, plagioclase and smaller quantities of quartz, opaques, epidote, calcite and actinolite. The primary texture is grano-nematoblastic. It is obliterated by hydrothermal activity, which gives it the characteristics of a propylite. It is crossed by epidote and calcite mesofractures and secant metasomatic veins on the foliation, that transform the amphiboles. One of the mesofractures with monomineral epidote composition contains asbestos fibers. The metasomatic veins, ranging from around 10 to around 100 microns, are older than the epidote and calcite vein. Plagioclases are sericitized, giving plagioclase crystals a turbid appearance in plane light. When they are crossed by the metasomatic vein, they recrystallize and have no more sericite. The quartz is poikilitic when it is observed with cross-polarized light (CPL). Unorganized subgrains appear, which may be related to a cataclastic deformation. Amphiboles are very elongated in the foliation. They are pleochroic, varying from blue-green to yellow-brown compatible with hornblende. They have quartz, plagioclase and epidote inclusions. At the intersection of the metasomatic vein and the amphiboles, a secondary mineral that is actinolite is observed (phase A) as a pseudomorph after the hornblende (figure 1a). Contact between the actinolite and the hornblende is rectilinear. Subgrains (phase B) individualize in the actinolite with boundaries generally parallel to the cleavage (110). Under pressure from the

hydrothermal fluid which, in this sample, results in interstitial quartz crystallization, subgrains can break off and create new grains. Subgrains and secondary grains vary greatly in size. Subgrains are 1-10 microns wide, and vary in length from a few microns to 100 microns. Their length depends on the width of the vein and the space between the microcracks that transect them. In this sample, phase A is marked by the nature of the vein and its sharp edges and the fact that the actinolites in the vein have the same extinction as the unaltered hornblendes in the parent rock. Phase B is marked by highly visible cleavages in the actinolite and the individualization of the subgrains. Phase C begins with the start of fracturation separation of a small block of DSGs.

Sample ALP2 is a propylite made up of very long altered actinolite, plagioclase, quartz epidote, and calcite. The rock is crossed by mesofractures, one of which is plurimillimetric. Its monomineral core is made up of epidote. Its borders contain quartz, calcite and asbestiform actinolite. On the walls of the mesofracture, BPAMs can be observed (figure. 1b) taking root in the DSGs (phases C and D).

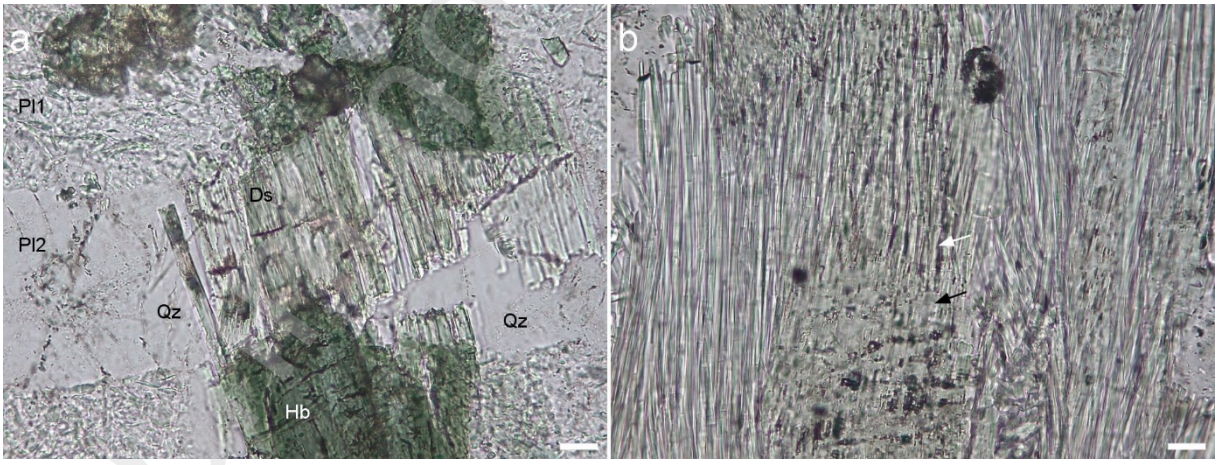

Figure 1: Observation under a plane polarized light microscope, bar = 20 microns; a) Sample ALP1, individualization of actinolite subgrains in a metasomatic vein and the early stage of fracturation Pl1: primary plagioclase, Pl2 secondary plagioclase, Qz: quartz, Hb: hornblende, Act: actinolite (phase A, B and C); b) Sample ALP2, development of BPAMs, white arrow, DSGs, black arrow (phase C and D).

The second example (sample COR) is an ante-Alpine amphibolite from Cap Corse altered by hydrothermal circulations, probably Alpine. This rock is mainly made up of brown hornblende. It contains smaller quantities of actinolite, quartz, epidote, chlorite, apatite and opaques. The primary rock has a granular texture. It is obliterated by hydrothermal activity, which gives it the characteristics of a propylite. The thin section was cut from a part of the rock that includes the end of a mesofracture full of quartz and that contains irregular secant metasomatic veins on amphibole phenocrysts where subgrains form. The mesofracture contains asbestos actinolite. Metasomatic veins from 10 to 100 microns wide are older than the quartz-filled cracks. The oldest veins are from phase A. They are about 10 microns wide. Actinolite is observed as a pseudomorph after the hornblende, when these narrow veins cross the amphiboles. In these veins (figure 2a) the actinolite cleavage marks are comparable to the hornblende cleavage marks. They are, however, well marked (figure 2b) in wider veins of about 100 microns where subgrains individualize, that are sometimes separated by epidote, evidence of microcirculations of fluids from phase B. In these veins, the actinolite subgrains for the most part have an extinction angle of 13°, as do the hornblendes. In other metasomatic zones (figure 2c) DSGs can be very thin and very long. Those in figure 2c are about 0.9 microns wide and 13 microns long. The depth, however, may be considerable. Phase C can be observed in different fossilized microfractures. In one microfracture (figure 2d) measuring 300 microns long and 120 microns wide, quartz has crystallized. It contains a large amount of actinolite debris; for the most part only the section of this debris is visible. A debris section generally measures less than one micron. The source of this debris should not be far, because DSGs of actinolite on the walls of the microfracture were, for the most part, broken during the opening under hydrothermal fluid pressure. The

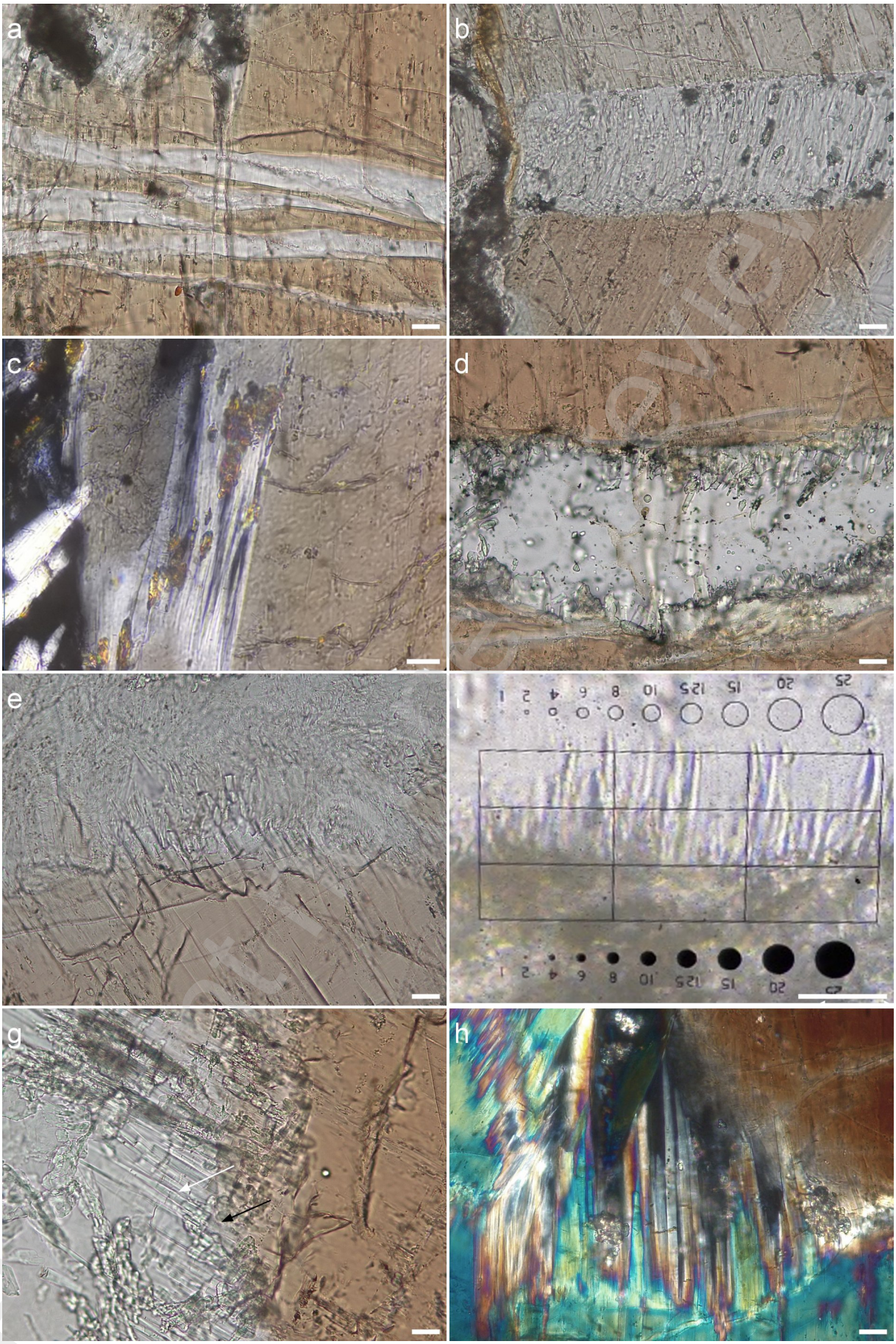

Figure 2 : Sample COR collected Around a meso-fracture pit, observations under a plane polarized light microscope except for image h which was observed under cross polarized light, bar = 20µm; a) Actinolites form pseudomorphs after magnesio-hornblendes in the metasomatic process (phase A); b) Actinolites form pseudomorphs after magnesio-hornblendes in a metasomatic vein. Subgrains individualize (DSGs) under fluid pressure, as evidenced by epidote precipitation (phase B); c) DSGs can be very thin after dissolution activity. Epidote precipitation indicates that fluids flowed through the mineral and that components conducive to precipitation were transported further away (phase B); d) A sudden inflow of fluid in the microfracture breaks the subgrain. A large amount of debris is trapped in the quartz during its precipitation (phase C); e) Very thin BPAMs develop from the broken DSGs. Quartz precipitated in the interstices left by the BPAMs on the edges of the mesofracture, (phase C and D); f) Early-stage growth of BPAM in a microfracture, the significant presence of epidote makes it difficult to observe DSGs (phase D); g) Conical BPAM, white arrow, that develops from a truncated DSG, black arrow (phase D); h) Microcavity filled with highly developed conical BPAM, with very thin BPAMs around the base, some epidotes serving as evidence of hydrothermal fluid circulation (phase D).

extremities of the DSGs are very irregular and can form the substrate for asbestiform mineral nuclei. Actinolite debris may also serve as a substrate for nuclei. Broken DSGs (figure 2e) (phase C) can be observed along the edge of the quartz vein. The fracture surface is very irregular and stimulates asbestiform mineral nucleation. We can see the expression of phase D in a quartz-filled microfracture where BPAMs (figure 2f) are beginning to grow. These actinolites are conical in shape with a base measuring around 2.5 microns on average, an apex of 1 micron and an aspect ratio of 7.12, the width being taken as the average between the base and the peak. Epidote has completely invaded the base of the BPAMs, infrequent DSG apexes of the same width as the BPAMs can be seen. Another microfracture includes BPAMs (figure 2g) that grow from the DSG apexes. Some BPAMs are conical with smooth walls. They have microcracks perpendicular to their longest axis. The growth of these minerals is more advanced than the previous minerals. We can make the same observation in the microcavities (figure 2h).

The third example is a sample (VEN) of dolerite from the Vendée department dating from before the Devonian period that transects the Bourneuf formation, which is assumed to be Cambrian. We can recognize the intergranular doleritic texture in the sample; however, the rock was obliterated by hydrothermal activity, which gives it the characteristics of a propylite. It is mainly made up of plagioclase, actinolite and smaller quantities of chlorite and epidote. It is crossed by quartz veins containing asbestos

actinolite, see previous publication (LAHONDERE 2018). The plagioclases are altered. The amphiboles are all altered and transformed into actinolite. Epidote appears in clusters distributed over the entire section. There are patches of chlorite with epidote inclusions often associated with the quartz around the edges of the mesofractures. In this sample, it is mainly phase D that can be seen locally on the wall of a mesofracture (figure 3a) containing asbestos fibers, in an area that was sheltered from the flow of hydrothermal fluids; BPAMs are starting to develop. These are cones of growth on top of DSGs. Interstitial quartz contains a large amount of actinolite debris. BPAMs are between 1.1 and 17 microns wide on average. Their lengths vary between 2.8 and 42 microns. The aspect ratio ranges from 1.4 to 3.3. At the apex of the widest cones, smaller cones form. They range from 1 to 3 microns wide. It is difficult to measure the dimensions of DSGs because they are generally partially covered by actinolite growth. In another sheltered area (figure 3c) on the wall of the mesofracture, BPAMs have very different widths. BPAMs are rooted in altered amphiboles. Their average widths are between 0.9 and 5 microns, the ratio between the base and the apex ranges from 1.3 to 6 and they are from 4.9 to 70 microns long. Their aspect ratio ranges from 3.1 to 24. Most BPAMs are split at a microcrack that cuts the mineral There are very many microcracks. DSGs are visible sometimes extended by a BPAM along the C axis. DSGs are from 0.35 to 4.5 microns wide and from 7 to 14 microns long. Their aspect ratio ranges from 2.8 to 40. Their length is controlled by microcracks cutting across the DSGs. This sample shows the effect of a sudden change in fluid pressure during asbestos actinolite growth (figure 3d). The BPAMs are rooted in an altered actinolite that shows DSGs that are locally well marked. The BPAMs are extended by fibers of under one micron. Some BPAMs are broken. The BPAMs and their fibrous ends were laid flat in the flow and were stuck in that position when the quartz crystallized. A large

amount of debris can be observed in a sheltered area formed by the altered actinolite. Most of the phenomena described on the walls of the mesofractures can be observed in the microfractures of the damage zone, which is around 1 cm, example the growth cones. (figure 3b)

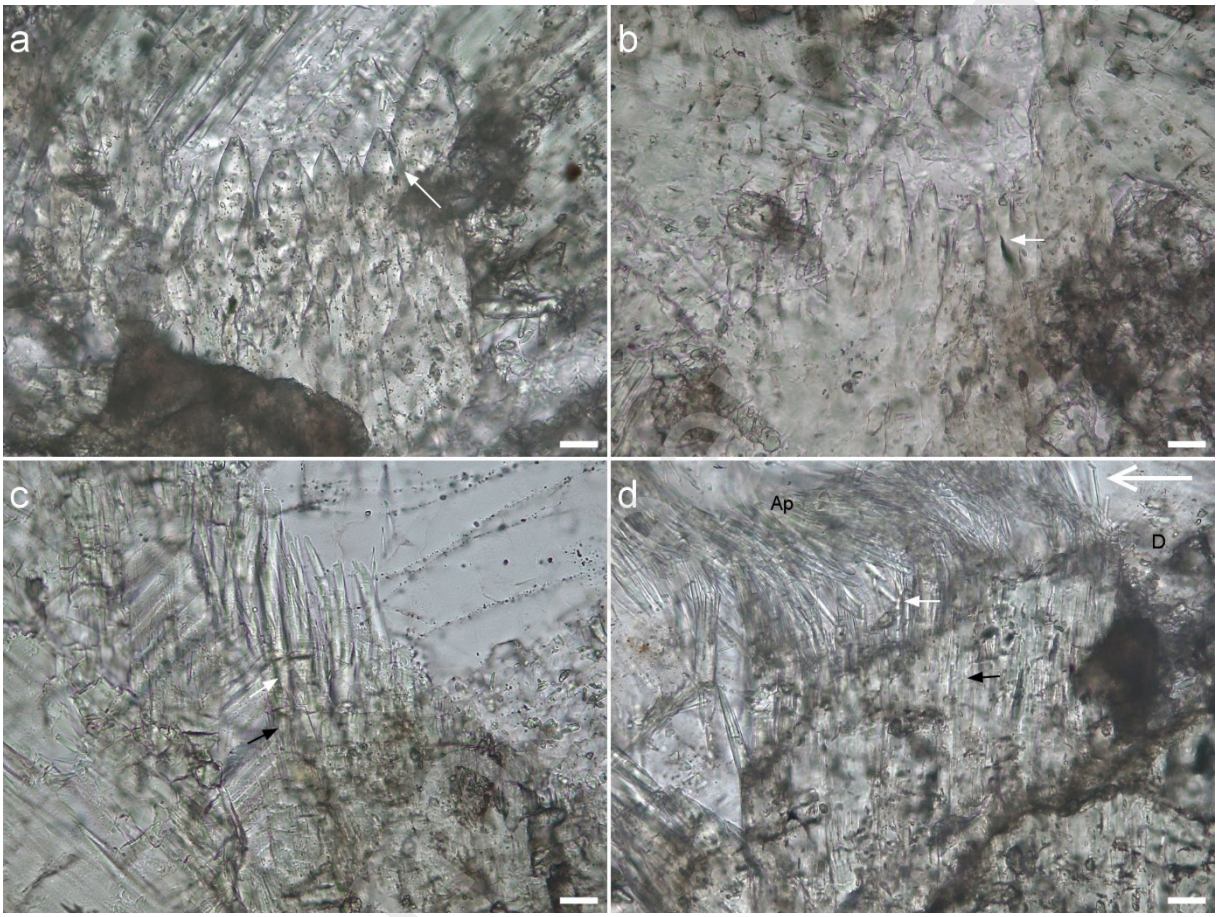

Figure 3 : Sample VEN, observations under a plane polarized light microscope, bar = 20µm, BPAMs, white filled arrows, phase D; a) Growth of conical actinolite BPAMs on the wall of a mesofracture; b) Growth of conical BPAMs in a 1 cm microfracture of the mesofracture; c) In a zone sheltered from the flow of hydrothermal fluid on a mesofracture wall, most BPAMs (white filled arrow) are split at a microcrack that cuts the mineral, DSGs, black filled arrow; d) The expression of the impact of a change in hydrothermal fluid flow on actinolite asbestiform minerals was fixed in place by the quartz precipitation on the walls of a mesofracture, direction of flow, white open arrow, broken BPAMs, white filled arrow, Ap, apical part of curved asbestiform minerals, D, debris, DSGs, black filled arrow.

The sample (PYR) from the fourth example was taken from skarns in the Salau Mine in the Pyrenees. The Salau skarns arise from a relationship between an intrusive igneous rock, pluton, and surrounding carbonate rocks. The intrusion of igneous rocks (mainly Granodiorite) dates back to the Carboniferous Period during the Hercynian episode. For more details see previous work (MISSERI 2021). The sample analyzed is a

303 mix of pieces of metasomatic rock of around one centimeter dispersed in a matrix made
304 up of sulfide mineralization. “U/Pb dating on hydrothermal apatite collected in these
305 sulfides yields an age of 289 ± 2 Ma” (POITRENAUD, 2018). Overall, this rock is
306 characterized by a wide-ranging composition. Within the sulfide mineralization, we can
307 see clinopyroxene, scheelite and calcite crystals. In the metasomatic rock pieces
308 spread throughout the mineralized sulfide gangue, we find: clinopyroxene skarns and
309 propylites containing epidote, quartz, plagioclase, amphiboles (siliceous
310 ferrohornblende and ferroactinolite), clinozoisite, chlorite and opaques. The skarns
311 have a granular texture. The siliceous ferrohornblende is mainly prismatic, sometimes
312 very highly altered and corroded. It can be found in inclusions in the sulfides, or
313 associated with the epidote or calcite. A small quantity of ferroactinolites appears in
314 the form of fibers (300/5 microns) included in quartz grains. Quartz, calcite and epidote
315 form monomineral clusters with a cataclastic texture. Quartz can also appear in the
316 form of porphyroclasts with a rolling extinction and surrounded by smaller-sized
317 neoblasts. There is an area on the thin section where ferrohornblendes and
318 ferroactinolites are prismatic, very altered and corroded (figure 4a). The corrosion is
319 so extensive that the DSGs have very irregular edges. These amphiboles are the
320 expression of phase B. The development of the sulfides, calcite and epidote means
321 that contacts with the skarns are not visible, making it impossible to collect information
322 on phase A. Microcavities can be seen in the altered amphiboles. Some are filled with
323 calcite and/or quartz. This is evidence of fracturation, which leads to microcavity
324 coalescence and promotes hydrothermal fluid circulation (phase C). Some of these
325 microcavities show BPAM nuclei (figure 4b) or the growth of BPAMs from DSGs (figure
326 4c). There are infrequent microfractures (phase D) where we can see the growth of
327 BPAMs that are thinner than DSGs. Nucleation starts from a fracture plane. This plane

is highly irregular. The presence of debris in the quartz phenocrysts is evidence of a high degree of variation in the pressure of the hydrothermal fluid that caused the DSGs and BPAMs to break. No apical part of asbestiform minerals was observed in these phenocrysts. (figure 4d).

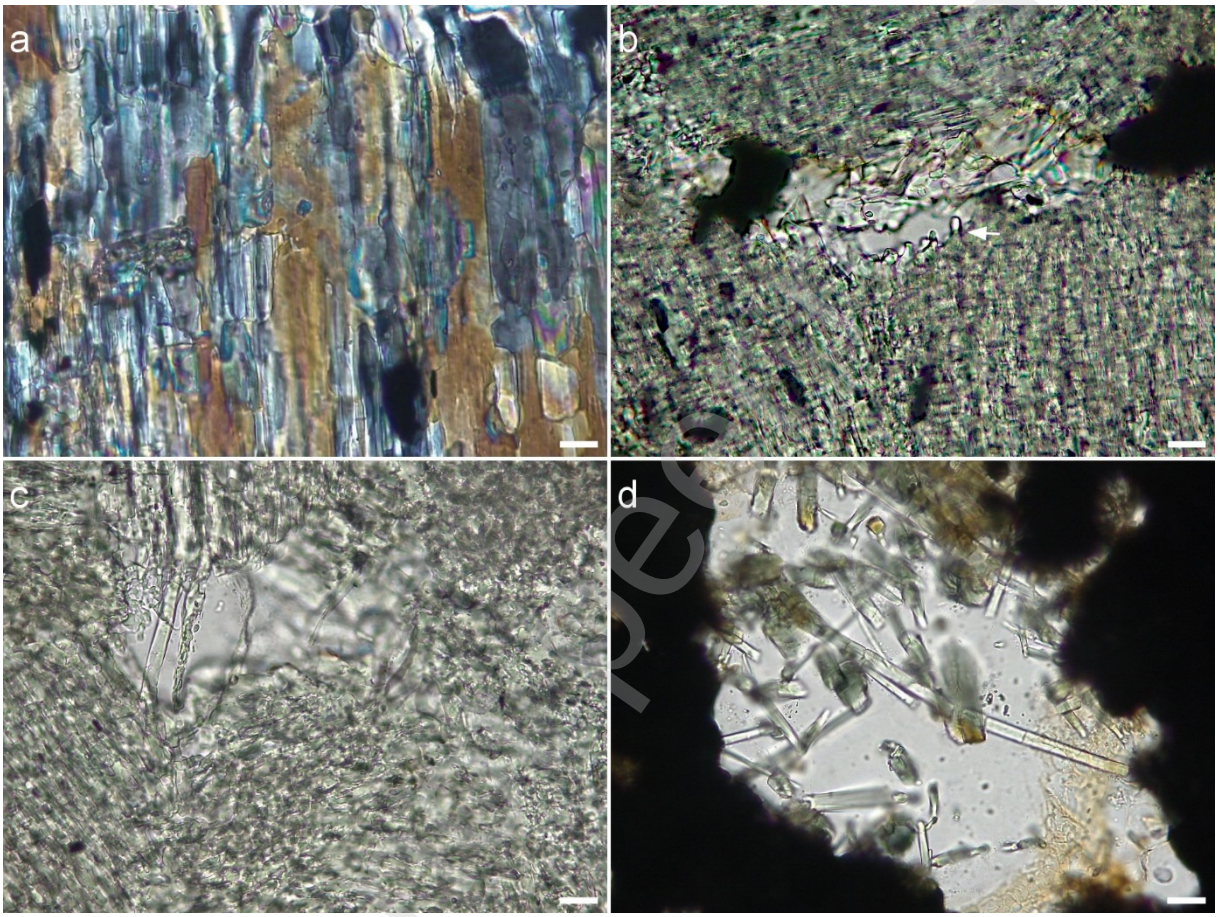

Figure 4 : Sample PYR, observations under a plane polarized light microscope except for image which was observed morphological similarities with the weathering-altered amphiboles. It contains numerous microcavities (phase B); b) BPAMs nuclei in a microfracture with island growth-type morphology. The microcavity is partially filled with quartz and calcite (phase C); c) BPAM development in a quartz-filled microcavity (phase C); d) BPAMs and DSGs fragments in a quartz phenocryst surrounded by metallic sulfide (phase D).

3.2. Results from TEM observations

Each of the two samples observed by TEM contain a particle where DSG-BPAM contact can be seen.

The first particle comes from New Caledonia greenschist (sample NC). This particle (figure 5a) is morphologically complex. It shows two BPAMs that developed from a

fragment of tremolite. The morphology of the fragment could not be determined, because only a part is visible. The longest BPAM is slightly conical with a diameter of 2 microns at its base. It contains many dislocations at its base. The second BPAM develops from a fragment of actinolite that has a cone-shaped end.

The second particle comes from asphalt road aggregate (sample GR). This is a fiber which, though thin, has a shape that is compatible with a BPAM (figure 5b). It is slightly conical with a diameter of 0.25 microns at its base. It grows from a parallel-edge DSG with a diameter of 0,95 microns.

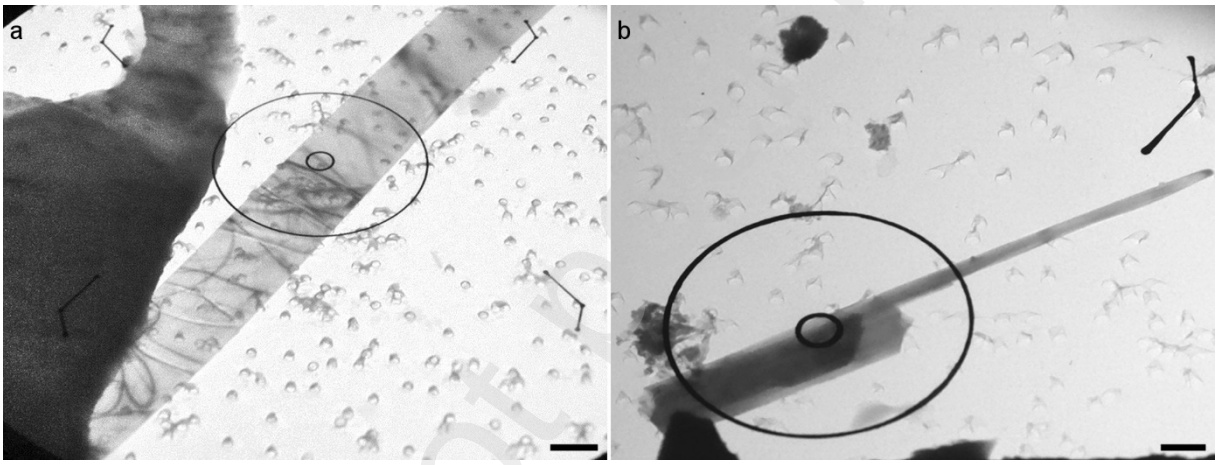

Figure 5 : TEM observations, fragments with contact between DSG and BPMA, a) Sample NC, fragment of tremolite from New Caledonia greenschist, bar = 0,96 µm, b) Sample GR fragment of actinolite from Asphalt road aggregate, bar = 0,6µm.

3.3. Discussion

The most useful observations for the asbestiform mineral formation study were made, as expected, on mesofracture pit zones. Namely, in the second example. There were fewer observations along the mesofractures. This is likely due to successive fracturations of the rock that destroy the actinolites or due to the fact that actinolites are particularly obscured by the precipitation of minerals such as epidote.

The process of asbestiform mineral nucleation and development is independent of the nature of the rocks studied. Namely, amphibolites, dolerites and skarns that were transformed into propylites and that have in common the fact that they contain partially altered hornblendes.

The nucleation process appears to begin (phase A) with the local pseudomorphic transformation of hornblendes into actinolite. Secondary amphiboles preserve original morphology. According to Putnis (PUTNIS, 2002), “pseudomorphs are a clear example of dissolution-precipitation” and they require interaction between a fluid and the parent mineral in order to develop. The fact that this phenomenon was only clearly observed in the example two sample may mean that it develops more particularly in the propagation zone in front of the mesofractures and that it is subsequently obliterated by the other phases of mesofracture progression. It is also possible for phase B to come very quickly after phase A.

In phase B, actinolite resulting from pseudomorphosis changes appearance. The cleavages are very marked and subgrains individualize (DSG). Some authors talk about fibrous actinolite to describe these minerals (AUSTIN, 2019) or actinolite-tremolite “with acicular to fibrous morphology compatible with the “asbestos” definition” (LUCCI, 2018). Generally, in this phase, there is little to no evidence of new actinolite precipitation. It is likely that the individualization is due either to fracturation caused by fluid pressure on the altered actinolite, or to a dissolution of the altered actinolite by the fluid along the cleavage planes, or to a combination of the two.

Subgrain individualization caused by fluid pressure activity in an amphibole may be exacerbated in phase C after fracturation and before the growth of new amphiboles. Sample LIM is an amphibolite from the Limousin region crossed by a thin fracture

measuring several microns that contains quartz and calcite. Several microfractures are present in this sample. The development of subgrains in one of these microfractures (figure 6) is a good illustration of this phenomenon. In this microfracture, there is no obvious trace of hydrothermal mineral precipitation other than that of the quartz. Given the appearance of the amphibole, it was affected by partial dissolution probably caused by fluid pressure on the walls of the microfracture. The fluid acts as a wedge that splits the wood. It uses cleavage fragments as one way of penetrating the amphiboles. This phenomenon individualizes DSGs. The shallowest dissolution planes isolate subgrains that can be very thin (less than one micron). This phenomenon has not been as clearly observed in the samples studied, probably because these subgrains were covered by new generations of actinolite precipitations. The fact remains that these subgrains are serious candidates when it comes to forming substrates for the nuclei of the thinnest asbestiform minerals. DSGs may have very different morphologies. Their morphologies have much in common with those described for the dissolved parts of weathered amphiboles (VELBEL, 2007), for example, stalactite/stalagmite-like (figure 2c). The most altered actinolites contain microcavities (figure 4a), indicating extensive dissolution.

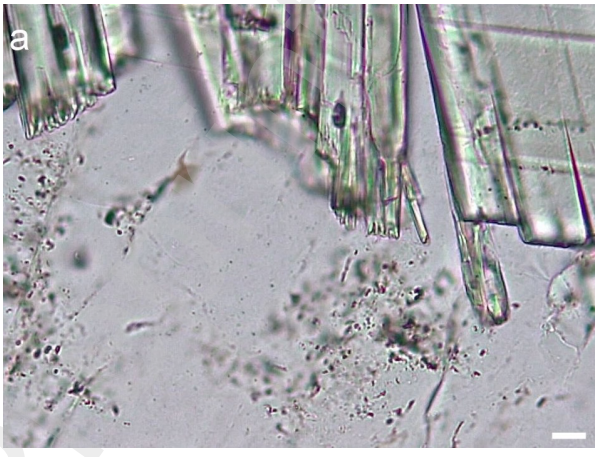

Figure 6 : Microfracture in the sample LIM: Formation of subgrains in an amphibole, bar = 7,5, µm.

According to ISO 10312 (2019), a cleavage fragment is a fragment of a crystal that is bounded by cleavage faces. It is difficult to consider subgrains that individualize after dissolution and/or fracturation of prismatic or acicular actinolite before any entropic interventions as potential cleavage fragments. When there is major hydrothermal alteration, subgrains are heavily corroded and generally inconsistently thinned. Under certain physical and chemical conditions, the surface of these faces may become amorphous (ZHANG, 2015). Under pressure from the fluid, subgrains can naturally transform into elongated actinolite grains that are very thin at less than one micron wide. The term DSG was selected for this article because the part of the grain that will become a subboundary then an elongated actinolite grain gradually changes morphology. DSGs spend a large part of this transformation closely bound by their base to the actinolite porphyroclasts they come from. This is why they have the same extinction as the porphyroclasts when observed under CPL. They are also connected to other DSGs that come from the same cleavages. In this case, individualization can be assessed by the interference color, which shifts towards first-order colors as DSGs individualize.

DSGs can be broken very close to their base by the force of a microfracture opening and the sudden inflow of fluid (phase C, figure 2d). The shape of the fracture is very irregular. Adjoining DSGs were broken along planes that are not at the same level. The fracture creates surfaces subperpendicular to axis C of the DSG, which can be very thin. These surfaces can also stimulate BPAM nucleation. These BPAMs develop along the extension of axis C of the underlying DSG (figure 2e). Morphology of the fracture is comparable to that observed for a tensile fracture of carbon fibers in a laminated composite (GREENHALGH 2009). Destroyed fragments of the DSGs are carried away by the fluid and some may serve as asbestiform mineral

nuclei. At this stage, two processes can cause nucleus substrate to form: dissolution and fracturation. Given the nature of the DSG-BPAM contacts, fracturation is the primary process. This does not prevent dissolution from contributing before fracturation to the reduction in the DSG-BPAM contact surfaces.

A BPAM nucleus (phase D), based on the observations made in the fourth sample, appears in the form of a drop on a cone with a very wide base (figure 4b) that grows out of a highly corroded DSG. “The observed nucleus has an island growth type morphology,” (DUBROVSKII, 2009). BPAMs at a more advanced stage of growth have a distinctive shape with a subcylindrical base, a slightly cone-shaped upper portion and a slightly rounded apex (figure 2f, 2g, 2h). These morphologies are not described in articles that discuss “hydrothermally synthesized” ferroactinolite (JENKINS, 2003; ERNSTE, 1966) or tremolite (DELLA VENTURA, 2003; BLOISE 2008). Hydrothermal synthesis uses no nucleus to start development and the first steps in growth cannot be observed. Similar morphologies have, however, been described for “growing whisker nanocrystals using the mechanism Vapor–Liquid–Crystal (VLC)” (GIVARGIZOV, 1973; DUBROVSKII, 2009; DUBROVSKII 2006). This process requires a substrate of the same type as the mineral produced, as well as the presence of impurities to stimulate nucleation. Some observations show that fluids do not necessarily remain in their entirety and that only a part of the fluid precipitates (epidote, calcite, quartz) in the microfractures (figure 2h, 4b). Fluids are probably sporadically present in the microfractures and mesofractures and intermittent circulation of gas cannot be ruled out. BPAM formation by natural vapor phase homoepitaxy is possible. According to other authors, however, when “the nucleation of fibers from the vein walls is in correspondence of truncated mafic

minerals the dominant process is dissolution-diffusion-crystallization" (ANDREANI, 2005; VIGNAROLI, 2020).

For the most part, BPAMs contain microcracks that are subperpendicular to axis C. In the thin section of example 3 (figure 3d) a change in hydrothermal fluid flow breaks BPAMs and not the apical parts of asbestiform minerals. This indicates that BPAMs are more rigid than the apical parts of asbestiform minerals and that BPAMs are probably not clusters of fibers. Fractured BPAMs can be carried away by flows (figure 4d) after fracturation.

The mineralogical boundary between asbestiform minerals and altered prismatic or acicular minerals in the examples described is the boundary between DSGs and BPAMs. This boundary can be established to within a few microns when doing a thin section study by PLM. It is, however, harder to differentiate particles resulting from human activity on DSGs or BPAMs. Depending on the degree of dissolution, particles from DSGs may have widths comparable to those of the thickest BPAMs. DSGs and BPAMs will preferentially break at the microcracks and they can have comparable aspect ratios. There is significant dimensional overlap between these two types of particles. This means other criteria should be used to differentiate. Observation by PLM on thin section is done in only two dimensions. The interference color gives information on DSG and BPAM thickness. For both, the interference color gradually shifts towards first-order colors. For DSGs, this is based on the degree of dissolution, while BPAMs are thicker at the base. Overall, BPAMs are less thick. This is confirmed when contact between both forms of actinolite can be observed by TEM (figure 5a and b), as BPAMs are more transparent. BPAMs

may be tube-shaped, cone-shaped or slightly cone-shaped and their edges are regular. Although this is not the objective of this article, we have observed that BPAMs (figure 3c) in most cases, have multiple successive divisions of thinner and more flexible fibers as we move towards their extremities. Divisions seem to occur at microcracks. By PLM, in some cases, the BPAM extinction angle can decrease by several degrees compared to DSGs. Towards the extremities, more and more fiber clusters have parallel extinction. This is likely due to preferential development of bundles in the apical portion of asbestiform minerals.

The process which leads to the formation of the Apical Part of Asbestos Minerals (APAMs) can be interrupted in Example 4; only BPAMs are observable. The hydrothermal alteration which is the cause is pre-Carboniferous while on the same site another phase of post or late Hercynian hydrothermal alteration was completed with the growing of APAMs (MISSERI 2021).

It is possible that the asbestos formation mechanism observed in calcium amphiboles is the same in magnesium-iron-manganese amphiboles. The shapes observed in some samples suggest that this is the case see the photo figure 7

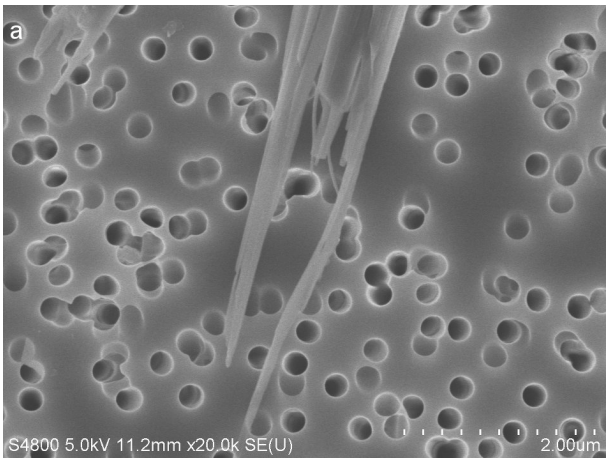

Figure 7 : photo credit: Martin Harper, SEM, anthophyllite (Dadeville, Alabama) with growing minerals looking like calcium amphibole BPAM

Observations were made on extension fractures. They cannot necessarily be transposed to other types of fractures.

4. Conclusion

The description of the steps that precede asbestiform mineral nucleation and the start of their development has allowed us to highlight the following points.

In high-temperature propylites containing hornblendes, when physical and chemical conditions are right, hydrothermal circulation causes dissolution, leading to the formation of actinolite or ferroactinolite subgrains, DSGs. Human mechanical activity on DSGs will produce particles with a different morphology from that of the prismatic or acicular amphibole cleavage fragments.

Natural hydraulic fracturation causes the creation of small surface areas at the extremities of the DSGs of actinolite which stimulates nucleation. The nuclei and some BPAMs do not have the same morphology as the APAMs. The same is true for particles that are produced after human mechanical activity.

Knowing the effect of the inhalation of particles from DSGs and BPAMs on health enables us to identify particles that should be considered to assess asbestos risk.

Since damage zones surround the fractures that contain asbestiform minerals, the presence of DSG particles in the ground material observed by PLM can be used as a precursor to excavation work.

This study concerns only calcium amphiboles. It would be interesting to study ferric and sodium amphiboles to check if this model can be applied to them.

Acknowledgments

This manuscript benefitted from criticisms and suggestions by Tomáš Daněk, The author would like to thank Patrick Bontemps, Thierry Leturcq, Gianpino W. Bianchi, Ivan R. Surace, Olivier Blein for the long lively discussions that sparked his interest in damage zones.

Funding sources

This work was supported by the French “Credit Impot Recherche” of AD-LAB that is dedicated to scientific research.

References

Andréani, M., Boullier, A. M., & Gratier, J. P. (2005). Development of schistosity by dissolution–crystallization in a Californian serpentinite gouge. *Journal of Structural Geology, 27(12)*, 2256-2267. https://doi.org/10.1016/j.jsg.2005.08.004

Austin, T. (2019). Petrogenesis of Unusual Occurrence of Amphibole Asbestos in Mohave County, Arizona and Clark County, Nevada (Doctoral dissertation, University of Nevada, Las Vegas).

Bazant, Z. P. (2003). *Fracture Mechanics of Concrete Structures: Proceedings of the First International Conference on Fracture Mechanics of Concrete Structures (FraMCoS1), held at Beaver Run Resort, Breckenridge, Colorado, USA, 1-5 June 1992.* CRC Press. https://doi.org/10.1201/9781482286847

Bailey, K. F., Kelse, J., Wylie, A. G., & Lee, R. J. (2004). The asbestiform and prismatic mineral growth habit and their relationship to cancer studies: A pictorial presentation.

Berman, D. W. (2003). *Analysis and Interpretation of Measurements for the Determination of Asbestos Core Samples Collected at the Southdown Quarry in Sparta, New Jersey.* Aeolus, Incorporated.

Bloise, A., Fornero, E., Belluso, E., Barrese, E., & Rinaudo, C. (2008). Synthesis and characterization of tremolite asbestos fibres. *European Journal of Mineralogy, 20(6),* 1027-1033. https://doi.org/10.1127/0935-1221/2009/0021-1838

Chatfield, E. J. (2008, July). A procedure for quantitative description of fibrosity in amphibole minerals. *In 2008 Johnson Conference: critical issues in monitoring asbestos, ASTM International, Burlington, Vermont.*

Choi, J. H., Edwards, P., Ko, K., & Kim, Y. S. (2016). Definition and classification of fault damage zones: A review and a new methodological approach. *Earth-Science Reviews, 152,* 70-87. https://doi.org/10.1016/j.earscirev.2015.11.006

Dubrovskii, V. G., Cirlin, G. E., & Ustinov, V. M. (2009). Semiconductor nanowhiskers: synthesis, properties, and applications. *Semiconductors, 43(12)*, 1539-1584. https://doi.org/10.1134/S106378260912001X

552 Dubrovskii, V. G., Soshnikov, I. P., Sibirev, N. V., Cirlin, G. E., & Ustinov, V. M. (2006).
553 Growth of GaAs nanoscale whiskers by magnetron sputtering deposition. *Journal of*
554 *crystal growth, 289(1)*, 31-36.

555 Ernst, W. G. (1966). Synthesis and stability relations of ferrotremolite. *American*
556 *Journal of Science, 264(1)*, 37-65. https://doi.org/10.1016/j.jcrysgro.2005.10.112

557 Givargizov, E. I. (1973). Oriented growth of whiskers and plate crystals of CdSe on
558 CdSe substrates. In *Doklady Akademii Nauk* (Vol. 211, No. 2, pp. 332-335). Russian
559 Academy of Sciences.

560 Greenhalgh, E. S. (2009). *Failure Analysis and Fractography of Polymer Composites*.
561 Elsevier.

562 Harper, M., Lee, E. G., Doorn, S. S., & Hammond, O. (2008). Differentiating non-
563 asbestiform amphibole and amphibole asbestos by size characteristics. *Journal of*
564 *occupational and environmental hygiene, 5(12),* 761-770.
565 http://dx.doi.org/10.1080/15459620802462290

566 HSG 248 (2021) *Asbestos: The analysts' guide, Health And Safety Executive Books.*

567 ISO 22262-1(2012) *Air quality - Bulk materials - Part 1: Sampling and qualitative*
568 *determination of asbestos in commercial bulk materials.*

569 ISO ISO 13794 (2019) *Ambient air - Determination of asbestos fibres - Indirect-transfer*
570 *transmission electron microscopy method d'amiante par microscopie électronique à*
571 *transmission - Méthode indirecte.*

572 ISO 10312 (2019) *Ambient air - Determination of asbestos fibres - Direct transfer*
573 *transmission electron microscopy method*.

574 ISO 14966 (2019) Ambient air - *Determination of numerical concentration of inorganic*
575 *fibrous particles - Scanning electron microscopy method*.

576 Jenkins, D. M., & Bozhilov, K. N. (2003). Stability and thermodynamic properties of
577 ferro-actinolite: a re-investigation. *American Journal of science, 303(8),* 723-752.
578 https://doi.org/10.2475/ajs.303.8.723

579 Kim, Y. S., Peacock, D. C., & Sanderson, D. J. (2004). Fault damage zones. *Journal*
580 *of structural geology, 26(3)*, 503-517. https://doi.org/10.1016/j.jsg.2003.08.002

581 Lahondère, D., Cagnard, F., Wille, G., Duron, J., & Misseri, M. (2018). TEM and
582 FESEM characterization of asbestiform and non-asbestiform actinolite fibers in
583 hydrothermally altered dolerites (France). *Environmental Earth Sciences*, *77(10),* 1-22.
584 https://doi.org/10.1007/s12665-018-7549-5

585 Lucci, F., Della Ventura, G., Conte, A., Nazzari, M., & Scarlato, P. (2018). Naturally
586 occurring asbestos (NOA) in granitoid rocks, a case study from Sardinia (Italy).
587 *Minerals*, *8(10),* 442. https://doi.org/10.3390/min8100442

588 Misseri, M., & Billon-Galland, M. A. (2021). Established Cases of the Development of
589 Asbestos-Related Lung Diseases in Miners at the Salau Tungsten Mine in France Due
590 to Exposure to Asbestos Actinolite and Asbestos Ferro-Actinolite. *Asbestos and Other*
591 *Elongate Mineral Particles—New and Continuing Challenges in the 21st Century*, 31-
592 61. http://doi.org/10.1520/STP163220200048

593 Misseri, M., & Lahondere, D. (2018). Characterisation of chemically related asbestos
594 amphiboles of actinolite: proposal for a specific differentiation in the diagram (Si apfu
595 versus Mg/Mg+ Fe2+). *International Journal of Metrology and Quality Engineering*, 9,
596 16. https://doi.org/10.1051/ijmqe/2018014

Mohammadnejad, M., Liu, H., Chan, A., Dehkhoda, S., & Fukuda, D. (2021). An overview on advances in computational fracture mechanics of rock. *Geosystem Engineering*, *24*(4), 206-229. https://doi.org/10.1080/12269328.2018.1448006

NF X43-050 (2021) Qualité de l'air - *Détermination de la concentration en fibres d'amiante par microscopie électronique à transmission - Méthode indirecte.* AFNOR, Normes nationales et documents normatifs nationaux.

Peacock, D. C. P., Dimmen, V., Rotevatn, A., & Sanderson, D. J. (2017). A broader classification of damage zones. *Journal of Structural Geology*, *102*, 179-192. https://doi.org/10.1016/j.jsg.2017.08.004

Perkins, R. L., & Harvey, B. W. (1993). Method for the determination of asbestos in bulk building materials (test method) (p. 112). EPA-600/R-93/116: 51-54.

Poitrenaud, T. (2018). *Le gisement périgranitique à tungstène et or de Salau (Pyrénées, France), histoire polyphasée d'un système minéralisé tardi-varisque* (Doctoral dissertation, Université d'Orléans).

Putnis, A. (2002). Mineral replacement reactions: from macroscopic observations to microscopic mechanisms. *Mineralogical Magazine*, *66*(5), 689-708. https://doi.org/10.1180/0026461026650056

Stanton, M. F., Layard, M., Tegeris, A., Miller, E., May, M., Morgan, E., & Smith, A. (1981). Relation of particle dimension to carcinogenicity in amphibole asbestoses and other fibrous minerals. *Journal of the National Cancer Institute*, *67*(5), 965-975.

Van der Wel, D. (1972). Asbestos minerals from Kongsberg silver deposit. *Norsk Geologisk Tidsskrift*, *52*, 287-294.

619 Van Mier, J. G. (1996). *Fracture processes of concrete* (Vol. 12). CRC press.

620 Van Orden, D. R., Lee, R. J., Allison, K. A., & Addison, J. (2009). Width distributions of
621 asbestos and non-asbestos amphibole minerals. *Indoor and Built Environment*, *18*(6),
622 531-540. https://doi.org/10.1177/1420326X09341503

623 Van Orden, D. R., Allison, K. A., & Lee, R. J. (2008). Differentiating amphibole asbestos
624 from non-asbestos in a complex mineral environment. *Indoor and Built Environment*,
625 *17*(1), 58-68. https://doi.org/10.1177/1420326X07087006

626 Ventura, G. D., Hawthorne, F. C., Robert, J. L., & Iezzi, G. (2003). Synthesis and
627 infrared spectroscopy of amphiboles along the tremolite-pargasite join. *European*
628 *Journal of Mineralogy*, *15*(2), 341-347. https://doi.org/10.1127/0935-1221/2003/0015-
629 0341

630 Vignaroli, G., Rossetti, F., Billi, A., Theye, T., & Belardi, G. (2020). Structurally
631 controlled growth of fibrous amphibole in tectonized metagabbro: constraints on
632 asbestos concentrations in non-serpentinized rocks. *Journal of the Geological Society*,
633 *177*(1), 103-119. https://doi.org/10.1144/jgs2018-235

634 Velbel, M. A. (2007). Surface textures and dissolution processes of heavy minerals in
635 the sedimentary cycle: examples from pyroxenes and amphiboles. *Developments in*
636 *Sedimentology, 58*, 113-150.

637 Von Richthofen, F. F.(1868) *natural system of volcanic rocks* (Vol. 1). Towne and
638 Bacon, printers.Sciences, 1, part. 2, p.1-94.

WHO (1997). *Determination of airborne fibre number concentrations: a recommended method, by phase-contrast optical microscopy (membrane filter method)*. World Health Organization.

Zhang, X., Zhang, R., & Hu, S. (2015). Experimental study of dissolution rates of actinolite in CaCl2–HCl–H2O up to 400° C. *Journal of Asian Earth Sciences*, *110*, 201-220. https://doi.org/10.1016/J.JSEAES.2015.02.020

ZharikovF, V. A. (2007). 9. Metasomatism and metasomatic rocks. *A classification of metamorphic rocks and glossary of terms. Recommendations of the International Union of Geological Sciences Subcommission on the Systematics of Metamorphic Rocks*.